On the Fisher Identifiability of Coupled Transport Processes in Animal Hypoxia Experiments

Eman M. Abdelazim[1] and Hosam K. Fathy[2]

***Abstract*— This paper examines the Fisher identifiability of two coupled transport processes with substantial disparities in their transport coefficients. This work is motivated by the problem of estimating the efficacy of a novel life support technology for respiratory failure patients. The idea is to circulate an oxygen carrier through the patient's abdomen, thereby utilizing abdominal gas diffusion for life support. The paper presents a third-order nonlinear model of the coupled dynamics of gas transport in the lungs and abdomen during this medical intervention. Linearizing this model and exploiting time scale separation to reduce it to a first-order model makes it possible to gain fundamental insights into its parameter identifiability. The main insight is that the stronger transport process in the lungs acts as a feedback mechanism that weakens the identifiability of the parameter governing the weaker abdominal transport process. Manipulating the stronger transport process through active control and/or passive design can, therefore, potentially improve identifiability. The paper concludes by illustrating these insights using Monte Carlo simulation, showing a fourfold improvement in abdominal transport coefficient estimation accuracy through simple experimental redesign.**

I. Introduction

This paper examines the problem of estimating the parameters associated with two coupled transport processes. The paper addresses the following fundamental questions: *Suppose there is a significant disparity in the transport coefficients associated with these processes. How does this disparity affect the identifiability of the smaller/weaker coefficient? Moreover, is it possible to employ feedback control and/or experimental setup redesign to improve this identifiability?*

The above questions are broadly applicable to different domains including, for instance, parameter estimation for coupled heat transfer processes. In the context of this particular paper, the motivating question is associated with the development of a novel ventilation technology for respiratory failure. Respiratory failure occurs when a patient's lungs can no longer perform their main functions - namely, blood oxygenation and carbon dioxide clearance - without external life support. Addressing respiratory failure is a critical societal challenge, one example being the fact that more than 100,000 patients are hospitalized annually with acute respiratory distress syndrome (ARDS) in the U.S. alone [1].

Two treatment technologies currently exist for respiratory failure: mechanical ventilation and extracorporeal membrane oxygenation (ECMO). Both technologies suffer from significant complications and limitations. Mechanical ventilation increases the risk of lung damage through oxygen toxicity, barotrauma, etc. [2]. This has the potential to cause ventilator-induced lung injury (VILI), which increases the need for mechanical ventilation, creating a potentially fatal positive feedback loop. ECMO is a costly intervention that requires constant monitoring by medical professionals [3], and whose many associated complications include the risk of blood clotting [4]. This paper is motivated by a novel third potential life support technology for patients with respiratory failure - namely, peritoneal oxygenation. The idea, sketched in Fig. 1, is to perfuse (i.e., circulate) an oxygenated carrier through the patient's peritoneal (i.e., abdominal) cavity. This has the potential to enable the diffusion-based transport of oxygen from the into the patient's bloodstream. This provides additional oxygen to the patient, and also helps rest the lungs, thereby potentially helping them heal.

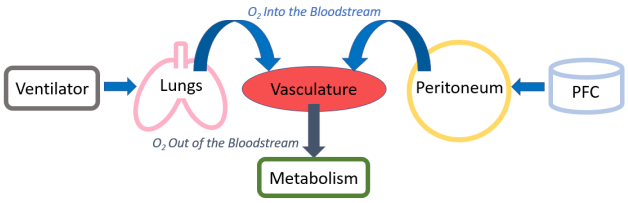

Fig. 1: Illustration of coupled transport processes

The literature presents a number of studies on peritoneal oxygenation, for different laboratory animals, using different oxygen carriers [5], [6], [7], [8], [9], [10]. This paper is motivated by the authors' ongoing experimental research on the peritoneal perfusion of a particular gas carrier - namely, an oxygenated perfluorocarbon (PFC) - in laboratory swine. Companion papers describe a novel mechatronic setup built for this research [11], as well as state-space models of the underlying dynamics of oxygen transport, carbon dioxide transport, and perfusion-induced abdominal pressure buildup [12], [13], [14]. A critical challenge in such state-space modeling efforts is the difficulty of accurately parameterizing the dynamics of peritoneal gas transport. The overarching goal of this paper is to analyze this difficulty and explore potential remedies for it. Specifically, the paper explores three fundamental questions motivated by peritoneal oxygenation but broadly applicable to other coupled transport estimation problems. First, how accurately can one estimate the parameters governing peritoneal oxygenation or other coupled transport processes? Second, how is this accuracy affected by the relative strengths of the underlying transport processes? Finally, how can one potentially manipulate these transport processes to improve estimation accuracy?

[1]Ph.D. student in Mechanical Eng., Univ. of Maryland, College Park. Email: emagdi@umd.edu
[2]Professor of Mechanical Eng., Univ. of Maryland, College Park. Email: hfathy@umd.edu

Preprint Received September 8, 2023 07:36:47 Pacific Time

The above questions are analyzed using Fisher identifiability analysis. This is an established tool in the estimation literature, with applications to various domains [15], [16], [17], [18]. To the best of the authors' knowledge, the application of Fisher analysis to coupled transport models with significant disparities in their underlying strengths is a novel addition to the literature. The remainder of this paper addresses this problem by making the following contributions. First, the paper integrates existing sub-models from the literature into a physics-based three-compartmental model of coupled transport in a peritoneal perfusion experiment. The model exhibits time scale separation, which makes it possible to residualize its underlying dynamics (Section II). Second, the paper applies Fisher information analysis analytically to a local linearization of this model (Section III). This furnishes fundamental insights regarding the model's parameter identifiability as well as the impact of perfusion experiment design on identifiability. Third, the paper uses Monte Carlo simulation to validate these insights numerically, for the original nonlinear three-compartment model (Section IV). Finally, Section V summarizes the paper's conclusions.

II. Coupled Transport Model

Consider the following three-compartment state-space model of a hypoxic laboratory animal experiencing peritoneal oxygenation, as shown in Fig. 1:

$$\begin{aligned}
\frac{d}{dt}\left(\frac{V_l x_1}{P}\right) &= u_1\left(u_2 - \frac{x_1}{P}\right) + QH_b(x_2 - f_d(x_1)),\\
\frac{d}{dt}(V_b H_b x_2) &= QH_b(f_d(x_1) - x_2) + \frac{\kappa A}{T}(x_3 - x_2) - w,\\
\frac{d}{dt}(V_p H_p x_3) &= u_3(u_4 - x_3) + \frac{\kappa A}{T}(x_2 - x_3).
\end{aligned} \tag{1}$$

The three state variables in the above model are the partial pressure of oxygen in the animal's lung compartment, $x_1(t)$, the fraction of dissolved oxygen in the animal's vasculature compartment, $x_2(t)$, and the fraction of dissolved oxygen in the PFC, $x_3(t)$. The function f_d represents the hemoglobin dissociation curve. The volumes of the lung, vasculature, and peritoneum compartments are V_l, V_b, and V_p, respectively. The symbol P represents the partial pressure of dry air, defined as the difference between atmospheric pressure, P_{atm}, and water vapor pressure, P_{H_2O}. The model's four input variables are the minute ventilation rate, $u_1(t)$, the fraction of inspired oxygen $u_2(t)$, the perfusion flowrate, $u_3(t)$, and the dissolved oxygen fraction in the PFC inflow, $u_4(t)$. The animal's metabolic oxygen consumption rate and total cardiac output are denoted by $w(t)$ and $Q(t)$, respectively, both of which are approximated as constant in this paper. The maximum solubility of oxygen is represented by H_b and H_p in the animal's blood and the PFC, respectively. Finally, κ represents diffusivity, A represents peritoneal surface area exposed to diffusion, and T represents the mean peritoneal diffusion distance/thickness.

Each state equation in the above model uses the law of mass conservation to relate the rate of change of stored oxygen in a given compartment to the corresponding oxygen transport and/or consumption rates. In the first state equation, for instance, the term $V_l x_l/P$ represents the volume of oxygen stored in the lung compartment, and accounts for the humidity of air inspired into the alveoli [19]. The term $u_1(u_2 - x_1/P)$ represents the advective transport of oxygen into and out of the lungs during inhalation and exhalation. The model approximates the alveolar and pulmonary venous partial pressures of oxygen as equal. This makes it possible to represent the transport of oxygen between the lung and vasculature compartments using the advective term $QH_b(x_2 - f_d(x_1))$ [20]. The function $f_d(x_1)$ in this term represents the relationship between the concentration and partial pressure of oxygen in the blood, also known as the *dissociation curve*. The literature presents multiple expressions approximating this dissociation curve, including the Hill and Adair equations [21]. This paper approximates the dissociation curve using the Hill equation [22], namely, $f_d(x_1) = ({x_1}^h)/(x_{150}^h + {x_1}^h)$. This equation's parameters are the cooperativity coefficient (h) and the oxygen partial pressure at 50% saturation (x_{150}). In the second state equation, the term $V_b H_b x_2$ represents the equivalent volume of oxygen (at standard temperature and pressure) stored in the blood. The term $\kappa A/T(x_2 - x_3)$ represents the rate of oxygen transport in the abdomen, based on Fick's law of diffusion [23]. Finally, in the third state equation, the term $u_3(u_4 - x_3)$ represents the advective exchange of dissolved oxygen between the abdominal cavity compartment and the external perfusion setup. Table I lists the nominal values of this model's parameters for a 55 kg pig, as well as the references used for estimating these values.

TABLE I: Nominal model parameter values

Parameter	Value	Parameter	Value
P	713 mmHg [24]	V_l	1.36 L [25]
H_b	184.65 mL_{O2}/L_{blood} [26]	V_b	3.685 L [27]
V_p	2 L [28]	H_p	403 mL_{O2}/L_{PFC} at 1 atm [29]
Q	5.86 L/min [30]	h	2.7 : 3 [31]
x_{150}	35.7 +/- 0.6 mmHg [32]	w	21.29 L_{O2}/hr [33]
A	10171 cm^2 [34]	T	316.9 $\pm$ 146.7 μm [35]
κ	7×10^{-6} :2×10^{-5} cm^2/s for 120 kg pigs [36]		

The above model can potentially be employed, together with animal perfusion experiment data, for assessing the efficacy of peritoneal oxygenation as a life support intervention. One way to achieve this goal is to estimate the model's parameters from experimental data, with a particular focus on estimating the effective peritoneal gas transport coefficient, $\kappa A/T$. This makes it important to evaluate the identifiability of $\kappa A/T$. The remainder of this paper performs this identifiability analysis twice, from both a theoretical perspective (in Section III) and a simulation perspective (in Section IV). Reducing the model's complexity simplifies the first (theoretical) analysis, and also helps contextualize it within the much broader framework of identifiability analysis for coupled transport processes beyond the specific application of peritoneal oxygenation. The remainder of this section simplifies the above state-space coupled diffusion model by *(i)* linearizing it around an

equilibrium point then *(ii)* residualizing the resulting linear model. The linearization process defines the model's state and input vectors as $\vec{x} = [x_1, x_2, x_3]^T$ and $\vec{u} = [u_2, u_4]^T$, respectively. This corresponds to an experimental setting where only the concentration of oxygen in both the inhaled air and the pumped PFC change with time. Given this choice of a smaller subset of input variables, one linearize the model around a desired/reference equilibrium to obtain:

$$\begin{aligned} \dot{x_1} &= \frac{u_{1e}}{V_l}(Pu_2 - x_1) + \frac{PQH_b}{V_l}(x_2 - Cx_1), \\ \dot{x_2} &= \frac{Q}{V_b}(Cx_1 - x_2) + \frac{\kappa A}{V_b H_b T}(x_3 - x_2), \\ \dot{x_3} &= \frac{\kappa A}{V_p H_p T}(x_2 - x_3) + \frac{u_{3e}}{V_p H_p}(u_4 - x_3), \end{aligned} \tag{2}$$

where C is a constant that equals $((x_1{}^{h-1})|_e/(x_{150}^h + x_1{}^h)|_e) - ((x_1{}^{2h-1})|_e/(x_{150}^h + x_1{}^h)^2|_e)$, and the subscript e denotes equilibrium.

The above model can be simplified further by exploiting the separation in time scales between its compartments. Specifically, because the dynamics of x_1 and x_3 are partially governed by advection and manifold filling, we assume that these dynamics are much faster than the dynamics of $x_2(t)$ for sufficiently large incoming flowrates $u_1(t)$ and $u_3(t)$. The values of $u_1(t)$ and $u_3(t)$, in this work, vary from 1-8 L/min and 1-6 L/min, respectively, leading to corresponding time constants of 10.2-81.9 s and 8-44.9 s for x_1 and x_3, respectively. The approximate time constant for x_2 is the inverse of $\kappa A/T$ which equals 106 s. This makes it plausible to residualize the model by approximating the dynamics of $x_1(t)$ and $x_3(t)$ as being instantaneous. The state variables corresponding to the residualized state equations are expressed as:

$$\begin{aligned} x_1 &= \frac{P}{u_{1e} + PCQH_b}(QH_b x_2 + u_{1e}u_2), \\ x_3 &= \frac{1}{\kappa A + Tu_{3e}}(\kappa A x_2 + Tu_{3e}u_4) \end{aligned} \tag{3}$$

Finally, the vasculature compartment is represented as:

$$\dot{x_2} = \frac{1}{V_b H_b}(L_1(PCu_2 - x_2) + L_2(u_4 - x_2)), \tag{4}$$

where, $L_1 = \frac{QH_b u_{1e}}{PC\left(\frac{u_{1e}}{PC} + QH_b\right)}$, and $L_2 = \frac{u_{3e}\frac{\kappa A}{T}}{u_{3e} + \frac{\kappa A}{T}}$.

Now this model can be simplified further and expressed as:

$$\dot{x} = k_1(\mu_1 - x) + k_2(\mu_2 - x), \tag{5}$$

where, $\mu_1(t) = PCu_2$, $x_2 = x$, $\mu_2(t) = u_4$, $k_1 = L_1/V_b H_b$, and $k_2 = L_2/V_b H_b$.

Eq. 5 is a first-order linear state equation relating the dynamics of an effective concentration, $x(t)$, to two effective input variables, $\mu_1(t)$ and $\mu_2(t)$. Thanks to its simplicity, analyzing this equation's identifiability can potentially guide a broad range of applications beyond peritoneal oxygenation.

III. Simplified Identifiability Analysis

This section applies Fisher identifiability analysis to the simple first-order linear coupled transport model shown in Eq. 5. Consider an experiment where the two transport coefficients, k_1 and k_2, are both unknown, but the primary goal is to estimate k_2. Moreover, suppose that this experiment involves setting the first control input $\mu_1(t)$ to zero while applying a step change to the second control input, $\mu_2(t) = U_o \mathscr{U}(t)$. Here, $\mathscr{U}(t)$ is the unit step function and U_o is the magnitude of this second input. Assuming zero initial conditions, the resulting trajectory for $x(t)$ is given by:

$$x(t) = \frac{U_o k_2}{\lambda}(1 - e^{-\lambda t}), \tag{6}$$

where, $\lambda = k_1 + k_2$. Suppose that the above trajectory of $x(t)$ is sampled uniformly in time, with some sampling time δt. Moreover, suppose that the resulting measurements of $x(t)$ are corrupted by a zero-mean, independent, identically distributed (i.i.d.) Gaussian noise process of variance σ_v^2. Then the output equation for the above experiment is:

$$y_k = U_o \frac{k_2}{\lambda}(1 - e^{-\lambda k \delta t}) + v_k, \tag{7}$$

where y_k and v_k are the measured output and measurement noise process value at time instant k, respectively. Consider the problem of simultaneously estimating k_2 and λ using a maximum likelihood approach. Fisher information analysis can provide a local approximation of the best parameter estimation accuracy that can be achieved by any unbiased solution to this problem. To perform Fisher analysis, begin by computing the sensitivities of the above output, without noise, to the two unknown parameters, as follows:

$$\begin{aligned} s_1(t) &= \frac{\partial(y_k - v_k)}{\partial k_2} = U_o \frac{1}{\lambda}(1 - e^{-\lambda t}) \\ s_2(t) &= \frac{\partial(y_k - v_k)}{\partial \lambda} = U_o \left[-\frac{k_2}{\lambda^2}(1 - e^{-\lambda t}) + \frac{k_2}{\lambda} t e^{-\lambda t} \right], \end{aligned} \tag{8}$$

Given the above sensitivities, one can compute the corresponding Fisher information matrix as follows:

$$\mathbf{F} = \frac{1}{\sigma_v^2} \begin{bmatrix} \sum_{k=1}^N s_1^2(k\delta t) & \sum_{k=1}^N s_1(k\delta t) s_2(k\delta t) \\ \sum_{k=1}^N s_1(k\delta t) s_2(k\delta t) & \sum_{k=1}^N s_2^2(k\delta t) \end{bmatrix}, \tag{9}$$

where N is the number of measurement instants during the given experiment. In the limit as the sampling time δt approaches zero, the above Fisher information matrix can be approximated using integrals instead of sums:

$$\mathbf{F} = \frac{1}{\delta t \sigma_v^2} \begin{bmatrix} \int_0^T s_1^2(t)dt & \int_0^T s_1(t)s_2(t)dt \\ \int_0^T s_1(t)s_2(t)dt & \int_0^T s_2^2(t)dt \end{bmatrix} \tag{10}$$

Finally, the Cramér-Rao theorem states that the best achievable parameter estimation error covariance is given by the inverse of the above Fisher information matrix, i.e., $\mathbf{C} =$

$\mathbf{F}^{-1}$. Computing this matrix analytically and focusing on the term corresponding to the parameter k_2 gives:

$$C(2,2) = \frac{-8\delta t\sigma_v^2\lambda^5 e^{2\lambda T}\begin{pmatrix}4e^{\lambda T}-3e^{2\lambda T}\\ +2\lambda T e^{2\lambda T}-1\end{pmatrix}}{U_o^2\begin{pmatrix}18k_2^2e^{2\lambda T}-32k_2^2e^{3\lambda T}+15k_2^2e^{4\lambda T}-k_2^2\\ -8\lambda T k_2^2 e^{\lambda T}+36\lambda T k_2^2 e^{2\lambda T}\\ -24\lambda T k_2^2 e^{3\lambda T}-4\lambda T k_2^2 e^{4\lambda T}\\ +12\lambda^2T^2k_2^2e^{2\lambda T}+8\lambda^3T^3k_2^2e^{2\lambda T}\end{pmatrix}} \tag{11}$$

Finally, consider an experiment whose duration is sufficiently long compared to the above system's characteristic time constant, $1/(k_1+k_2)$, to the point where it is reasonable to take the limit of the above Cramér-Rao bound as $T\to\infty$. For such an experiment, normalizing the above bound with respect to the square of the nominal value of k_2 gives:

$$\lim_{T\to\infty}\frac{\mathbf{C}(2,2)}{k_2^2} = \frac{24(k_1+k_2)^5\delta t\sigma_v^2}{15U_o^2k_2^2} \tag{12}$$

The diffusion coefficient k_1 only shows up in the numerator of the above equation. Therefore, as k_1 increases relative to k_2, the best variance with which one can estimate k_2 becomes progressively worse. This summarizes the paper's first main conceptual conclusion, namely, that as the diffusion coefficient corresponding to the stronger diffusion process increases, one's ability to estimate the coefficient corresponding to the weaker process diminishes. The above result makes intuitive sense in light of the fact that the term $k_1(\mu_1-x)$ in Eq. 5 can be construed as a negative feedback term pulling $x(t)$ towards $\mu_1(t)$. The transport coefficient k_1 can, therefore, be construed as a feedback gain whose large magnitude increases the sensitivity of $x(t)$ to $\mu_1(t)$ while decreasing the relative impact of both k_2 and $\mu_2(t)$ on $x(t)$. This sensitivity argument is quite visible in the Laplace domain, where the coupled transport dynamics are:

$$X(s) = \frac{k_1}{s+k_1+k_2}\mu_1(s) + \frac{k_2}{s+k_1+k_2}\mu_2(s) \tag{13}$$

The above expression shows that if $k_1\to\infty$ compared to k_2, then $X(s)$ is only influenced by $\mu_1(s)$ as its reference input without accounting for $\mu_2(s)$. This jeopardizes the degree to which one can estimate the weaker diffusion coefficient k_2. This raises an important possibility of using either active control or passive experimental redesign or both to recover and/or improve the identifiability of k_2. Specifically, consider the following target coupled transport dynamics:

$$\dot{x} = k_1'(\mu_1'-x) + k_2(\mu_2-x), \tag{14}$$

where μ_1' represents a new, fictitious input to the first transport process and k_1', is the corresponding effective diffusion coefficient. If k_1' is deliberately chosen to be much closer in value to k_2 compared to k_1, then the identifiability of k_2 will improve significantly. Matching this target model to the true plant dynamics involves solving for μ_1 as follows:

$$k_1(\mu_1-x) = k_1'(\mu_1'-x) \implies \mu_1 = \frac{k_1'}{k_1}\mu_1' + \frac{k_1-k_1'}{k_1}x \tag{15}$$

The above equation represents an active control law, incorporating positive feedback, where the control input, $\mu_1(t)$, governing the first transport process is deliberately manipulated to improve the identifiability of k_2. Positive feedback, in this case, helps improve parameter identifiability by attenuating the impact of the stronger transport process on the overall, coupled transport dynamics. In fact, in the limit as $k_1'\to 0$, the impact of the stronger diffusion process on overall system dynamics vanishes, and only the weaker transport process governs these dynamics. This can be achieved in practice by actively manipulating the control input, $\mu_1(t)$, to make it equal to the measured state, $x(t)$. In a peritoneal gas transport experiment, for instance, this can be achieved by manipulating mechanical ventilator settings to provide an inspired oxygen fraction that attenuates or eliminates transport gradients in the given laboratory animal's lungs.

Active control is not the only pathway for improving the Fisher identifiability of the parameter k_2. One can also manipulate the design of the perfusion experiment itself to improve identifiability. One way to do this is to adjust the equilibrium input values, u_{1e} and u_{3e}, around which the experiment is conducted. Three particular limit cases provide interesting insights regarding the impact of experiment design on the identifiability of k_2. For each of these cases, we compute the ratio k_1/k_2 and relate it to the physiological parameters of the three-compartment gas transport model, recalling that $k_1 = L_1/V_bH_b$, and $k_2 = L_2/V_bH_b$.

- In the case where both u_{1e} and u_{3e} are maximized (e.g., to provide maximum oxygenation to the animal), one can take the limits as u_{1e} & $u_{1e}\to\infty$, obtaining the following:

$$\lim_{u_{1e}\to\infty, u_{3e}\to\infty}\frac{k_1}{k_2} = \frac{QH_b}{\frac{\kappa A}{T}}, \tag{16}$$

  The above equation is undesirable in the sense that the ratio k_1/k_2 is dictated solely by physiological parameters outside the experimental designer's control. If the values of these physiological parameters cause the ratio k_1/k_2 to be large, then the identifiability of k_2 will be poor.
- In the case where u_{1e} is large but u_{3e} is small, one can take the limits $u_{1e}\to\infty$ and $u_{3e}\to 0$ to obtain:

$$\lim_{u_{1e}\to\infty, u_{3e}\to 0}\frac{k_1}{k_2} = \frac{QH_b}{u_{3e}} = \infty, \tag{17}$$

  This is an undesirable scenario where the ratio k_1/k_2 approaches infinity, and the identifiability of k_2 is lost.
- In case where u_{1e} is reduced to induce hypoxia while u_{3e} is increased to revive the animal, one can take the limits as $u_{1e}\to 0$ and $u_{3e}\to\infty$, obtaining:

$$\lim_{u_{1e}\to 0, u_{3e}\to\infty}\frac{k_1}{k_2} = \frac{u_{1e}}{PC\frac{\kappa A}{T}} = 0, \tag{18}$$

  which shows improved identifiability for $\kappa A/T$.

The above analysis shows that curtailing the equilibrium air flowrate into the lungs, u_{1e}, while maximizing the equilibrium PFC flowrate, u_{3e}, is particularly effective at increasing the identifiability of k_2. The next section validates this theoretical insight in simulation.

IV. Monte Carlo Simulations

This section constructs a Monte Carlo (MC) point cloud of model parameter estimates to validate the insights from the above analysis. This process starts with generating pseudo measurements from the nonlinear three-compartmental mathematical model using the parameters in Table I, then adding white noise to the model state x_2 to imitate having a noisy measured signal y. The pseudo measurements are produced for two cases of hypoxia experiments:

1) A *baseline case* representing a typical peritoneal oxygenation experiment, with $u_1 = 8$ L/min, $u_2 = 0.12$, and $u_3 = 1$ L/min.
2) An *illustrative "controlled" case* demonstrating the insights from this paper, where u_1 is curtailed to 1 L/min, u_2 increased to 0.3, and u_3 is set to 6 L/min.

For each of the above cases, the experimental protocol proceeds in two different steps. The first step is a one-minute interval where the animal goes to a hypoxic state from normoxia and the PFC concentration is zero (u_4 =0). The second step is an eleven-minute interval where there is a step change in the PFC concentration u_4 from 0 to 1 while the animal is hypoxic. After generating pseudo measurements, optimal estimation of the model parameters is performed using the maximum likelihood to estimate the following parameters: V_l, QH_b, V_bH_b, V_pH_p, w, and $\kappa A/T$. Finally, this is repeated a thousand times to generate an Monte Carlo point cloud estimate of the parameters as shown in Fig. 2. The mean of these parameter estimates is used to generate an optimized model response in both baseline and controlled cases as shown in Fig. 3. The white residuals between the response of the optimized model and the pseudo measurements shown in Fig. 4 indicate a good fit, reflecting the successful convergence of the estimator to unbiased parameter estimates. Table II summarizes the results of this optimization work by listing the nominal values and standard deviations of the point cloud estimates of both $k1$ and $k2$ for both the baseline and illustrative cases. The table also lists the ratios of the standard deviations obtained using the baseline experiment versus the illustrative experiment.

The above results are encouraging for at least four reasons. First, the results show that the accuracy with which one can estimate *both* $k1$ and $k2$ improves very substantially with a simple change in mechanical ventilator settings. Second, the results show that the fundamental insights gleaned earlier in this paper for a *linearized* model of the dynamics of hypoxia continues to hold for the full *nonlinear* model of these dynamics. Third, the fact that these improvements in identifiability were obtained for an illustrative experiment whose settings were guided by a theoretical study - but not optimized - suggests that optimal experimental design may potentially improve identifiability further. Fourth, it is interesting and encouraging to note that the time scale separation between the various compartment dynamics is significantly stronger for the baseline case compared to the illustrative one, but the insights regarding the potential improvements in identifiability continue to hold.

TABLE II: Statistical inference of MC parameters' estimates

Parameter	Nominal value	$\pm 3\sigma$ (baseline case)	$\pm 3\sigma$ (controlled case)	$\pm 3\sigma$ ratio
QH_b	1.082	3.778	0.268	14
$\kappa A/T$	0.385	0.239	0.0684	3.496

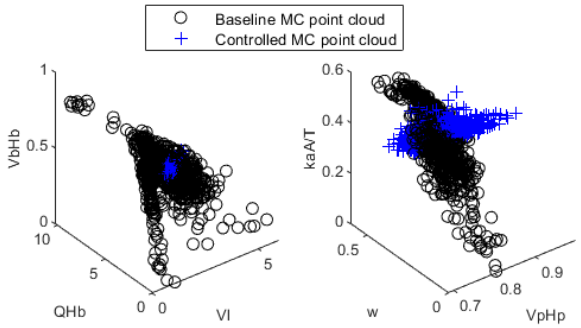

Fig. 2: The model parameter estimates for the uncontrolled and controlled pseudo experiments.

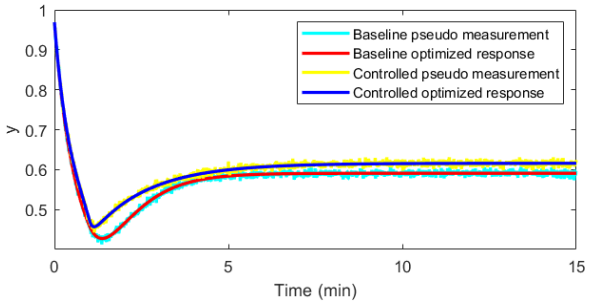

Fig. 3: The fitted model response of the pseudo measurements for baseline and controlled cases.

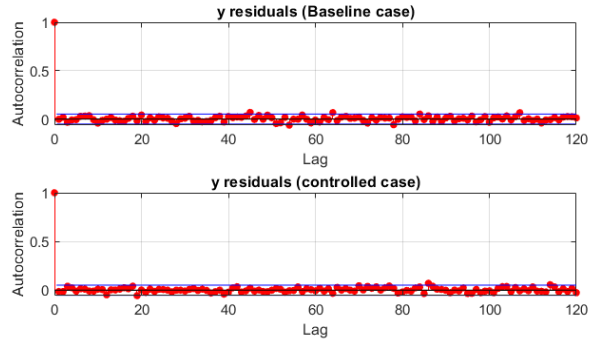

Fig. 4: The autocorrelation of residuals between the fitted model response and the pseudo measurements.

V. Conclusion

This paper constructs a nonlinear compartmental model of different oxygen transport mechanisms in hypoxic animals subjected to peritoneal oxygenation. This model is reduced to a linear 1^{st} order model representing two coupled transport processes. Fisher information identifiability analysis validated by Monte Carlo simulation proves improving the identifiability of the coefficient of the weaker transport process through positive feedback and manipulation of the

experimental inputs affecting transport coefficients to eliminate the huge difference between them. Future work includes the verification of these insights using experimental data.

ACKNOWLEDGMENTS

This research was funded by U.S. National Science Foundation Growing Convergence Research grant #2121110. The authors gratefully acknowledge this support.

REFERENCES

[1] E. Eworuke, J. M. Major, and L. I. G. McClain, "National incidence rates for acute respiratory distress syndrome (ards) and ards cause-specific factors in the united states (2006–2014)," *Journal of critical care*, vol. 47, pp. 192–197, 2018.

[2] A. Anzueto, F. Frutos-Vivar, A. Esteban, I. Alía, L. Brochard, T. Stewart, S. Benito, M. J. Tobin, J. Elizalde, F. Palizas *et al.*, "Incidence, risk factors and outcome of barotrauma in mechanically ventilated patients," *Intensive care medicine*, vol. 30, pp. 612–619, 2004.

[3] V. Mishra, J. L. Svennevig, J. F. Bugge, S. Andresen, A. Mathisen, H. Karlsen, I. Khushi, and T. P. Hagen, "Cost of extracorporeal membrane oxygenation: evidence from the rikshospitalet university hospital, oslo, norway," *European journal of cardio-thoracic surgery*, vol. 37, no. 2, pp. 339–342, 2010.

[4] D. A. Murphy, L. E. Hockings, R. K. Andrews, C. Aubron, E. E. Gardiner, V. A. Pellegrino, and A. K. Davis, "Extracorporeal membrane oxygenation—hemostatic complications," *Transfusion medicine reviews*, vol. 29, no. 2, pp. 90–101, 2015.

[5] S. R. Carr, J. P. Cantor, A. S. Rao, T. V. Lakshman, J. E. Collins, and J. S. Friedberg, "Peritoneal perfusion with oxygenated perfluorocarbon augments systemic oxygenation," *Chest*, vol. 130, no. 2, pp. 402–411, 2006.

[6] J. A. Feshitan, N. D. Legband, M. A. Borden, and B. S. Terry, "Systemic oxygen delivery by peritoneal perfusion of oxygen microbubbles," *Biomaterials*, vol. 35, no. 9, pp. 2600–2606, 2014.

[7] R. U. R. Mohammed, N. T. Zollinger, A. R. McCain, R. Romaguera-Matas, S. P. Harris, K. L. Buesing, M. A. Borden, and B. S. Terry, "Testing oxygenated microbubbles via intraperitoneal and intrathoracic routes on a large pig model of lps-induced acute respiratory distress syndrome," *Physiological Reports*, vol. 10, no. 17, p. e15451, 2022.

[8] J. Klein, N. S. Faithfull, P. J. Salt, and A. Trouwborst, "Transperitoneal oxygenation with fluorocarbons," *Anesthesia & Analgesia*, vol. 65, no. 7, pp. 734–738, 1986.

[9] N. Matsutani, B. Takase, Y. Nogami, Y. Ozeki, S. Kaneda, T. Maehara, M. Kikuchi, and M. Ishihara, "Efficacy of peritoneal oxygenation using a novel artificial oxygen carrier (trm-645) in a rat respiratory insufficiency model," *Surgery today*, vol. 40, pp. 451–455, 2010.

[10] J. Zhang, X. Wang, L. Wang, B. Xu, and M. Zheng, "Effect of oxygenation of transperitoneal ventilation on the death time after asphyxiation in rabbits." *Minerva anestesiologica*, vol. 76, no. 11, pp. 913–917, 2010.

[11] M. Doosthosseini, K. R. Aroom, M. R. Aroom, M. Culligan, W. Naselsky, C. Thamire, H. W. Haslach, S. A. Roller, J. R. Hughen, J. S. Friedberg *et al.*, "Monitoring, control system development, and experimental validation for a novel extrapulmonary respiratory support setup," *IEEE/ASME Transactions on Mechatronics*, vol. 27, no. 5, pp. 4177–4187, 2022.

[12] S. Wood, A. Commins, M. Doosthosseini, W. Naselsky, M. Culligan, K. Aroom, M. Aroom, B. Kadkhodaeielyaderani, Y. Moon, J. Leibowitz *et al.*, "Experimental parameterization of a model of hypoxia dynamics in yorkshire swine," *IFAC-PapersOnLine*, vol. 55, no. 37, pp. 752–757, 2022.

[13] M. Doosthosseini, Y. Moon, A. Commins, S. Wood, W. Naselsky, M. J. Culligan, K. Aroom, M. Aroom, A. Shah, G. J. Bittle *et al.*, "Estimating the impact of peritoneal perfluorocarbon perfusion on carbon dioxide transport dynamics in a laboratory animal," in *2022 American Control Conference (ACC)*. IEEE, 2022, pp. 3000–3005.

[14] N. Zaleski, Y. Moon, M. Doosthosseini, G. Hopkins, K. Aroom, M. Aroom, W. Naselsky, M. J. Culligan, J. Leibowitz, A. Shah *et al.*, "Modeling and experimental identification of peritoneal cavity pressure dynamics during oxygenated perfluorocarbon perfusion," in *2022 European Control Conference (ECC)*. IEEE, 2022, pp. 297–302.

[15] J. P. Norton, *An introduction to identification*. Courier Corporation, 2009.

[16] M. Gerdin, T. Glad, and L. Ljung, *Global identifiability of complex models, constructed from simple submodels*. Springer, 2007.

[17] G. Massonis, J. R. Banga, and A. F. Villaverde, "Structural identifiability and observability of compartmental models of the covid-19 pandemic," *Annual reviews in control*, vol. 51, pp. 441–459, 2021.

[18] A. Pozzi, G. Ciaramella, K. Gopalakrishnan, S. Volkwein, and D. M. Raimondo, "Optimal design of experiment for parameter estimation of a single particle model for lithiumion batteries," in *2018 IEEE Conference on Decision and Control (CDC)*. IEEE, 2018, pp. 6482–6487.

[19] S. Fuentes and Y. S. Chowdhury, "Fraction of inspired oxygen," 2020.

[20] C. E. Rhodes, D. Denault, and M. Varacallo, "Physiology, oxygen transport," in *StatPearls [Internet]*. StatPearls Publishing, 2022.

[21] I. A. Lavrinenko, G. A. Vashanov, J. L. H. Cáceres, and Y. D. Nechipurenko, "Fitting parameters of a modified hill's equation and their influence on the shape of the model hemoglobin oxygenation curve," *Oxygen*, vol. 3, pp. 90–101, 2 2023.

[22] D. P. Kaufman, P. F. Kandle, I. Murray, and A. S. Dhamoon, "Physiology, oxyhemoglobin dissociation curve," 2018.

[23] A. S. Popel, "Theory of oxygen transport to tissue," *Critical reviews in biomedical engineering*, vol. 17, no. 3, p. 257, 1989.

[24] S. Laukemper-Ostendorf, A. Scholz, K. Bürger, C. P. Heussel, M. Schmittner, N. Weiler, K. Markstaller, B. Eberle, H.-U. Kauczor, M. Quintel *et al.*, "19f-mri of perflubron for measurement of oxygen partial pressure in porcine lungs during partial liquid ventilation," *Magnetic Resonance in Medicine: An Official Journal of the International Society for Magnetic Resonance in Medicine*, vol. 47, no. 1, pp. 82–89, 2002.

[25] A. Rendas, M. Branthwaite, and L. Reid, "Growth of pulmonary circulation in normal pig–structural analysis and cardiopulmonary function," *Journal of Applied Physiology*, vol. 45, no. 5, pp. 806–817, 1978.

[26] J. L. Larimer, "Hemoglobin concentration and oxygen capacity of mammalian blood," *Journal of the Elisha Mitchell Scientific Society*, vol. 75, no. 2, pp. 174–177, 1959.

[27] J. P. Hannon, C. A. Bossone, and W. G. Rodkey, "Splenic red cell sequestration and blood volume measurements in conscious pigs," *American Journal of Physiology-Regulatory, Integrative and Comparative Physiology*, vol. 248, no. 3, pp. R293–R301, 1985.

[28] M. K. van Gelder, J. C. de Vries, F. Simonis, A. S. Monninkhof, D. H. Hazenbrink, G. Ligabue, S. Giovanella, J. A. Joles, M. C. Verhaar, M. A. Bajo Rubio *et al.*, "Evaluation of a system for sorbent-assisted peritoneal dialysis in a uremic pig model," *Physiological Reports*, vol. 8, no. 23, p. e14593, 2020.

[29] J. Jägers, A. Wrobeln, and K. B. Ferenz, "Perfluorocarbon-based oxygen carriers: from physics to physiology," *Pflügers Archiv-European Journal of Physiology*, vol. 473, pp. 139–150, 2021.

[30] L. Jivegård and J. Holm, "Cardiac output determinations in the pig–thoracic electrical bioimpedance versus thermodilution." *Critical care medicine*, vol. 18, no. 9, pp. 995–998, 1990.

[31] J. M. Mercer, "Cooperativity," in *Reference Module in Life Sciences*. Elsevier, 2023.

[32] D. C. Willford and E. P. Hill, "Modest effect of temperature on the porcine oxygen dissociation curve," *Respiration physiology*, vol. 64, no. 2, pp. 113–123, 1986.

[33] J. Van Milgen, J. Noblet, S. Dubois, and J.-F. Bernier, "Dynamic aspects of oxygen consumption and carbon dioxide production in swine," *British Journal of Nutrition*, vol. 78, no. 3, pp. 397–410, 1997.

[34] K. Kelley, S. Curtis, G. Marzan, H. Karara, and C. Anderson, "Body surface area of female swine," *Journal of animal science*, vol. 36, no. 5, pp. 927–930, 1973.

[35] J. C. de Vries, M. K. van Gelder, A. S. Monninkhof, S. Ahmed, D. H. Hazenbrink, T. Q. Nguyen, G. A. de Kort, E.-J. P. Vonken, K. R. Vaessen, J. A. Joles *et al.*, "A uremic pig model for peritoneal dialysis," *Toxins*, vol. 14, no. 9, p. 635, 2022.

[36] C. Androjna, J. E. Gatica, J. M. Belovich, and K. A. Derwin, "Oxygen diffusion through natural extracellular matrices: implications for estimating "critical thickness" values in tendon tissue engineering," *Tissue Engineering Part A*, vol. 14, no. 4, pp. 559–569, 2008.